IEEE Access
Multidisciplinary ⋮ Rapid Review ⋮ Open Access Journal

Received December 20, 2019, accepted February 2, 2020, date of publication February 7, 2020, date of current version February 20, 2020.

Digital Object Identifier 10.1109/ACCESS.2020.2972275

Fully Automatic Prediction for Efficacy of Photodynamic Therapy in Clinical Port-Wine Stains Treatment: A Pilot Study

SHENGNAN AI[1], CHENGMING WANG[1,2], WENXIN ZHANG[1], JUI-CHENG HSIEH[1], ZHENGYU CHEN[1], BIN HE[1], XIAO ZHANG[3], NING ZHANG[4], YING GU[5], AND PING XUE[1], (Member, IEEE)

[1]State Key Laboratory of Low-Dimensional Quantum Physics, Collaborative Innovation Center of Quantum Matter, Department of Physics, Tsinghua University, Beijing 100084, China
[2]Nuctech Company Limited, Beijing 100084, China
[3]School of Life Science, Beijing Institute of Technology, Beijing 100081, China
[4]Institute of Forensic Science, Ministry of Public Security, Beijing 100038, China
[5]Department of Laser Medicine, Chinese PLA General Hospital, Beijing 100853, China

Corresponding author: Ping Xue (xuep@tsinghua.edu.cn)

This work was supported in part by the National Natural Science Foundation of China under Grant 61227807, Grant 61575108, and Grant 61505034, and in part by the Tsinghua Initiative Scientific Research Program under Grant 2013THZ02-3.

ABSTRACT In this paper, we report a fully automatic method for the prediction of the treatment efficacy of photodynamic therapy during the clinical treatment in port-wine stains. Histogram of oriented gradients (HOG) features were extracted from optical coherence tomography images. Isolation forest (iForest) was used to build classifier based on these features, achieving a sensitivity of 84% and specificity of 91%. Our dataset consists of 336 PWS lesions of 121 patients. We aim to build a comprehensive computational model for the patients who respond positively to the photodynamic therapy, which could be used to sort and identify patients who respond poorly to photodynamic therapy before treatment and prevent them from unnecessary treatment.

INDEX TERMS Anomaly detection, machine learning, optical coherence tomography, port-wine stain, support vector data description.

I. INTRODUCTION

Port wine stain (PWS) is the congenital capillary dilation of skin, which occurs in 0.3% to 0.5% of the population [1]. The lesions are usually unilateral and about 75% to 80% occurs in the head and neck areas [2]. Most of the PWS lesions are benign. As the lesions do not regress spontaneously and deepen in color with age, patients' mental health could be significantly impacted [3]. Traditional therapies like freezing, surgical excision and tattooing are not used anymore, because they damage the skin and leave permanent scars after treatment [4]. Photodynamic therapy (PDT) was used to treat PWS in 1991 by Gu et al [5]. Good treatment results were got, as PDT can selectively destroy dilated vessels without damage to the normal skin [4]. However, during the diagnosis and treatment of PWS, there are still some problems. First, the diagnosis and treatment plan heavily relies on clinical judgement and clinician's experience. Second, there is no effective way to automatically sort and identify patients who rarely respond to the PDT before treatment, as standard PDT therapy is time-consuming, expensive and painful.

Optical coherence tomography (OCT) is a high-resolution, non-invasive, cross-sectional optical imaging modality first developed by Huang et al. in 1991 [6]. OCT has been widely used in various biomedical applications since then. Bowden et al. apply several machine learning algorithms to PS OCT images in detecting BCC [9]. Adabi et al. extract features from OCT images to generating a classifier of normal skin, then to identify skin diseases [10]. Singla et al extract quantitative features from OCT images to classify skin burns. In our previous publications, we proved that OCT could be a potential tool to monitor PDT treatment efficiency [6]–[8]. In clinical practice, most patients respond positively to PDT treatment while few patients rarely respond to PDT treatment [25], and patients who respond positively to PDT treatment are believed to have similarities [26].

The associate editor coordinating the review of this manuscript and approving it for publication was Sukhdev Roy.

Our recent work suggest that extracting quantitative features from optical coherence tomographic images could be a potentially powerful method for accurately and automatically identifying PWS margins during laser therapy [30]. In this work, we trained a classifier based on numerous features extracted from patients who respond positively, and then the classifier was used to identify patients who rarely respond. A total of 121 Chinese patients with PWS lesions on the face or neck areas participated in our research, among which 118 respond positively and 3 respond negatively. We extracted histogram of oriented gradients (HOG) features from OCT images. Isolation forest (iForest) was used to build the classifier. Sensitivity of 84% and specificity of 91% were achieved. To the best of our knowledge, this work is the first to develop a fully automated method to sort and identify patients who rarely respond to PDT treatment.

II. MATERIALS AND METHODS

A. OCT IMAGING COLLECTION

A time domain OCT systems (Beijing Newraysing Laser Tech Co. Ltd., Beijing, China) was used in this study as previous work described [7]. All image samples were collected from the Chinese PLA General Hospital as part of the standard-of-care treatment for PWS. The study protocol was approved by the PLA Postgraduate Medical School ethics board. 121 Chinese patients with PWS lesions on the face or neck areas participated in this study. From each patient, we collected one to seven tissue imaging samples.

B. DATASET CONSTRUCTION

The proposed algorithm followed several steps (visualized in Fig. 1). In ''image preprocessing'', image denoising and region of interest (ROI) selection were performed. In ''Feature extraction'', HOG features were extracted. Classifier based on iForest was trained on training dataset and was tested on testing dataset.

FIGURE 1. The overview of the algorithm.

1) IMAGING PREPROCESSING

Before feature extraction, images were preprocessed. A median filter with size of [3 3] pixels were used to eliminate speckle noise. Then the air-epidermis junction were recognized by regularized shortest path extraction [8]. After recognition, A-lines were shifted to make air-epidermis junction lay in the same level as the neighboring A-lines. Then the region 200 pixels below the air-epidermis was chosen as region of interest (ROI). The entire scan length of the system is 2.4 mm, with 400 pixels in axial direction [7]. The image depth of human skin is less than 1 mm (about 167 pixels in axial). Region deeper than 200 pixels along the axial direction was background, so we chose the region 200 pixels below the air-epidermis as ROI. The extracted surface and ROI are shown in Fig. 2. Further feature extractions are performed on the chosen ROI.

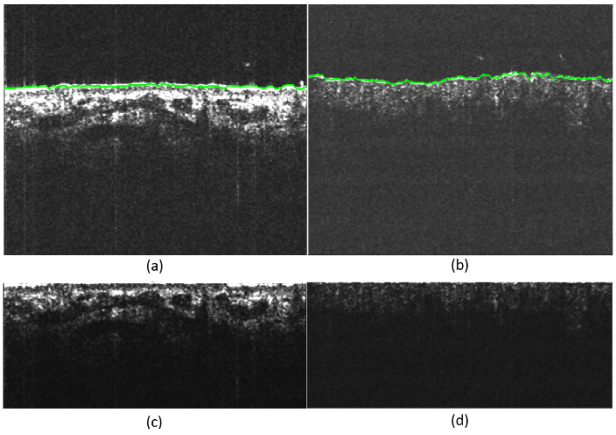

FIGURE 2. (a). A ''normal'' image after air-epidermis junction recognition; (b). An ''abnormal'' image after air-epidermis junction recognition; (c). ROI for a ''normal'' image after A-lines alignment; (d). ROI for an ''abnormal'' image after A-lines alignment.

2) HISTOGRAMS OF ORIENTED GRADIENT DESCRIPTORS

Histograms of oriented gradients (HOG) is a wildly used feature descriptor in object detection in computer vision and imaging processing. HOG can successfully detect local intensity gradients or edge directions in images. An image is divided into small connected portions called cells, and within each cell the number of gradient in each orientation is counted. Concatenation of these counts are called HOG descriptor [12]. As HOG feature descriptor can well describe the distribution of local intensity gradients and edge directions, researchers extract HOG feature descriptor from OCT images to train classifier in order to classify diseases automatically [13], [14]. In this paper, we extracted HOG features by using MATLAB command ''extractHOGFeatures''. The ROI was resized to [256 256], then divided to [8 8] cells. Each block has [2 2] cells. Between adjacent blocks, 2 cells were overlapped. In several scenarios, researchers build image

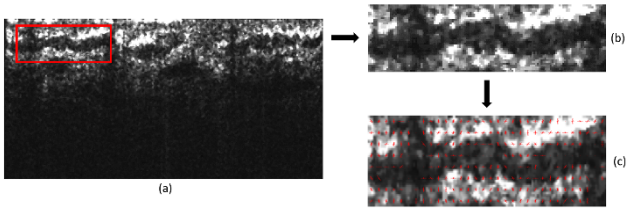

FIGURE 3. HOG features visualization. (a) Denoised, aligned ROI image; (b) cropped image part in the red box of (a); (c) HOG descriptor visualization for each block in (b).

pyramid to extract multiple scale features [13], while image pyramid was not applied as no accuracy improvement was achieved in our case.

C. BUILDING THE CLASSIFIER

After features extraction, an iForest classifier was trained. iForest is an unsupervised outlier detection method, which detects anomalies based on the isolation properties without distance or density measures [21]. This module works well in scenarios where exist a lot of ''normal'' instances and only a few ''abnormal'' instances. The ''normal'' instances are similar to one another. The ''abnormal'' instances are dissimilar to one another and to the ''normal'' instances as ''abnormality'' may be caused by various reasons. In these scenarios, most multi-class classification methods may not work well. In our case, iForest classifier is trained on ''normal'' instances to detect ''abnormal'' instances. After training, iForest can capture characteristics of ''normal'' instances, and distinguish ''abnormal'' instances as they have different characteristics. In our case, samples from patients who received PDT treatment for the first or second time with more than 20% color fades were treated as ''normal'' data. Samples from patient who received PDT treatment for above 10 times with no color fades were treated as ''abnormal'' data. Throughout our research project, patients do not fall into these two groups were not participated in our study. In clinical practice most patients were able to get more than 20% color fades during PDT treatment, the ''abnormal'' samples were very few [25]. Our data agree well with the clinical practice as ''normal'' data contains 118 patients with 324 image samples and ''abnormal'' data contains only 3 patients with 12 image samples.

III. RESULTS

In our dataset, there are 17640 HOG features. If all features are used for classifier training, a lot of time will be consumed. Principal component analysis (PCA) was used to reduce the feature scale. PCA is a statistical method that converts a large scale of variables to a smaller set of linearly uncorrelated variables called principal components [22]. All principal components are orthogonal to each other. The variance decrease progressively from the first to the last principal component [27]. A new set of variables were generated. Each new variable called principal component is a linear combination of the original variables and all new variables were orthogonal to each other. The first 323 variables were used as our new features. After PCA, the HOG features scale was reduced to 323. The number of major principal components was selected empirically.

After PCA, 323 features were used to train an iForest classifier. We used ten-fold-cross-validation to evaluate the accuracy. We randomly divided ''normal'' instances into ten subsets. Ten training iterations were performed. At each iteration, all ''abnormal'' instances together with one ''normal'' subset were used as testing set and the remaining nine ''normal'' subsets were used as training set. Anomaly detection by iForest included two stages: training and evaluation. In the training stage, 64 iTrees were constructed by recursively partitioning a subset from training set until all instances were isolated. For each iTree, a subset of 64 instances randomly selected without replacement from original training set were used for training. After training, an anomaly score was calculated for each training sample by equation (2). The value of anomaly score varies between 0 and 1. The higher the anomaly score, the more likely the instance would be an abnormal instance. All instances in the training set were ranked in descending order of anomaly scores. The anomaly score of the top 20% instance was used as threshold. If an instance had score higher than the threshold, the instance would be treated as ''abnormal'' instance. If an instance had score equal to or lower than the threshold, the instance would be treated as ''normal instance''. In our case, the threshold was chosen in order to get higher sensitivity value with specificity of 80% at least. On the training set, 80% of the instances were treated as ''normal'', and 20% of the instances were treated as ''abnormal''. The anomaly score was defined as follows [21]:

$$c(\varphi) = \begin{cases} 2H(\varphi-1) - \dfrac{2(\varphi-1)}{n} & for\ \varphi > 2 \\ 1 & for\ \varphi = 2 \\ 0 & otherwise \end{cases} \quad (1)$$

$$\text{score}(x, \varphi) = 2^{-\frac{E(h(x))}{c(\varphi)}} \quad (2)$$

where φ is the subsampling size. H(i) is the harmonic number and can be estimated by ln(i) + 0.5772156649. h(x) is a single path length from an iTree. c(φ) is the average of h(x) given φ. E(h(x)) is the average of h(x) from a collection of iTrees. The anomaly score of a particular instance can be calculated by equation (2).

Three parameters were calculated to evaluate our classifier: 1) accuracy, 2) sensitivity, 3) specificity. True positive (TP) is the number that ''abnormal'' patients classified as ''abnormal''. False positive (FP) is the number that ''normal'' patients classified as ''abnormal''. True negative is the number that ''normal'' patients classified as ''normal''. False negative is the number that ''abnormal'' patients classified as ''normal''. Sensitivity (also called the recall) measures the rate that true positive are correctly classified as positive. Specificity measures the rate that true negative are correctly classified as negative. Accuracy measures the rate that samples are correctly classified. These parameters can be calculated by following equations:

$$\text{sensitivity} = \frac{TP}{TP + FN} \quad (3)$$

$$\text{specificity} = \frac{TN}{TN + FP} \quad (4)$$

$$\text{accuracy} = \frac{TP + TN}{TP + FP + TN + FN} \quad (5)$$

Table 1 summarized the average accuracy, sensitivity and specificity on the testing set of ten iterations. The accuracy

TABLE 1. Summary of average accuracy, sensitivity and specificity.

	Accuracy	Sensitivity	Specificity
iForest	86%	91%	84%
SVDD	72%	8%	96%

of 86%, sensitivity of 91%, and specificity of 84% were achieved. The specificity of 84% on the testing set agree well with the specificity of 80% on training set. Sensitivity of 91% means that eleven out of the twelve ''abnormal'' instances were detected correctly by iForest classifier. The accuracy and sensitivity of detection are high, which means our classifier can be used to identify patients who rarely respond to the PDT before treatment.

The iForest results were compared with Support vector Data description (SVDD). Because of the data distribution in our case, the anomaly detection methods other than classification methods or regression methods are suitable for comparison. SVDD is anomaly detection method inspired by the Support Vector Classifier and has been used in a variety of applications. It obtains a closed boundary around a dataset and can be used to detect outliers from the dataset. In many instances these outliers has exceptionally large or small feature values compared to normal instances [28], [29]. SVDD solves the following optimization problem [29].

$$\begin{aligned} &\min_{R,a,\xi} R^2 + C\sum_{i=1}^{l}\xi_i \\ &\text{Subject to } \|\phi(x_i) - a\|^2 \le R^2 + \xi_i, \quad i = 1,\ldots,l, \\ &\qquad \xi_i \ge 0, \quad i = 1,\ldots,l, \end{aligned} \tag{6}$$

where, ϕ is the mapping function to a higher dimensional space, and C is the regularization parameter specified by user [28]. In our case, a Gaussian kernel was used. The ten-fold-cross-validation was used to evaluate the performance as iForest.

The iForest method built an ensemble of iTrees for a given dataset. Anomalies were those instances that few and different from normal instances, which called ''isolation''. Anomalies had short average path lengths on the iTrees. The SVDD method obtained a closed boundary around a training dataset. Anomalies were those instances that outside of the boundary. Often these anomalies show an exceptionally large or small feature value in comparison with other training instances [28], [29]. As a result of SVDD classification, instances with exceptionally large or small feature values would be detected as abnormal instances.

The results of SVDD were shown in table 1. The average accuracy of 72%, sensitivity of 8%, and specificity of 96% were achieved. With sensitivity of 8%, only one out of twelve ''abnormal'' instances were successfully detected by SVDD. SVDD is less accurate and much less sensitive than iForest. We believe that the significant difference in results obtained by these two algorithms on our dataset were caused by the distribution of the instances: 1) the anomaly instances were isolate from but close to the normal instances; 2) the feature values of anomaly instances were inside the value range of

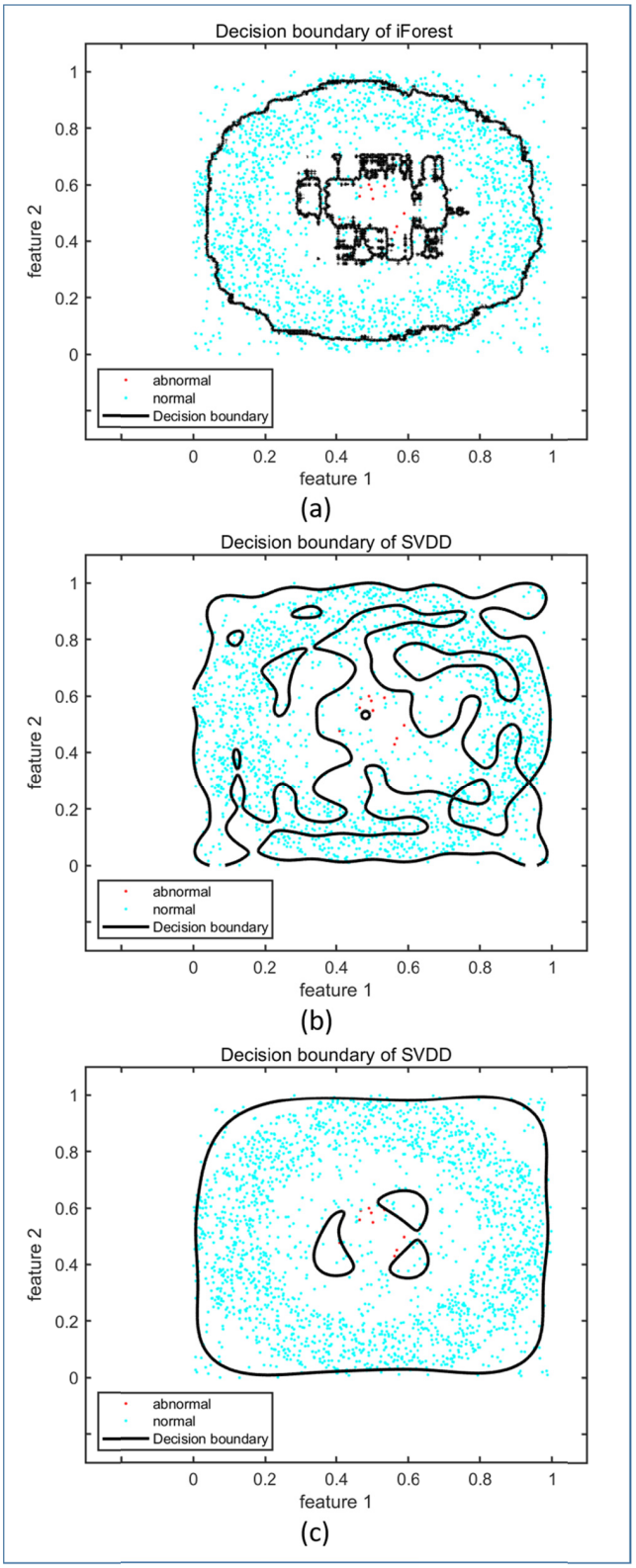

FIGURE 4. Toy example. (a) classification results of iForest; (b) classification results of SVDD with higher gamma; (c) classification results of SVDD with lower gamma.

the normal instances. A toy example was used for illustration. The instances of the toy example were generated randomly, following the above two distribution rules. Each instance of the toy example had two features, feature 1 and feature 2. As shown in Fig. 4, most of the normal instances were distributed on a thick ring, with inner radius 0.3 and outer radius 0.5. Only a few normal instances were distributed inside the inner edge or outside the outer edge of the ring. All abnormal instances have features neither too large nor too small and therefore were distributed inside the inner edge of the ring. Both iForest and SVDD were trained on the normal data and were tested on the abnormal data. As shown in Fig. 4 (a), the iForest algorithm was able to capture the properties of the data distribution. Most of the normal instances and abnormal instances were classified correctly. In our case, sensitivity of 91% and specificity of 84% imply that the normal data distribution is captured and the abnormal instances are identified correctly. Fig. 4 (b) and Fig. 4 (c) show the results of SVDD with higher gamma and lower gamma, respectively. With higher gamma, the SVDD is able to identify the abnormal instances, but fail to capture the properties of the data distribution. With lower gamma, the SVDD may capture the properties of the data distribution, but fail to identify the abnormal instances. In our case, the high specificity of SVDD classifier implies that the properties of the normal data distribution is captured, and the low sensitivity means that the abnormal instances cannot be correctly identified.

IV. CONCLUSION AND DISCUSSION

In clinical practice, most patients respond positively to PDT treatment while few patients rarely respond to PDT treatment [25]. This work is a pilot study to fully automatically sort and identify negatively responded patients for PDT treatment in PWS patients. In this paper, HOG features based on intensity OCT images were used. For the feature set, a comprehensive classifier for the PWS lesions which respond positively to the PDT treatment was build and used to identify the patients whose lesions respond negatively to the PDT treatment. In addition, our proposed workflow has the potential to be generalized to build classifiers for treatments of various disease.

The classification accuracy in this work may be further improved for clinical usage. Firstly, the data set is not large enough, and in the future we plan to collect more data. Secondly, all features were extracted from intensity images, and additional information like blood flow, polarization may help to improve the accuracy. Thirdly, the OCT system used in this work is a TD-OCT with lower SNR. In the future we plan to use SS-OCT system for data collection.

ACKNOWLEDGMENT

(Shengnan Ai and Chengming Wang contributed equally to this work.)

REFERENCES

[1] J. K. Chen, P. Ghasri, G. Aguilar, A. M. Van Drooge, A. Wolkerstorfer, K. M. Kelly, and M. Heger, "An overview of clinical and experimental treatment modalities for port wine stains," *J. Amer. Acad. Dermatol.*, vol. 67, no. 2, pp. 289.e29–304.e29, Aug. 2012.

[2] J. L. Finley, "Healing of port-wine stains after argon laser therapy," *Arch. Dermatol.*, vol. 117, no. 8, pp. 486–489, Aug. 1981.

[3] J. Wang, Y.-Y. Zhu, Z.-Y. Wang, X.-H. Yao, L.-F. Zhang, H. Lv, S.-P. Zhang, and B. Hu, "Analysis of quality of life and influencing factors in 197 Chinese patients with port-wine stains," *Medicine*, vol. 96, no. 51, Dec. 2017, Art. no. e9446.

[4] Y.-G. Lu, J.-J. Wu, Y.-D. Yang, H.-Z. Yang, and Y. He, "Photodynamic therapy of port-wine stains," *J. Dermatolog. Treat.*, vol. 21, no. 4, pp. 240–244, Art. no. 2010.

[5] G. Ying, L. Junheng, and S. Huanyan, "Clinical application of copper vapor laser in PDT for fifty cases of PWS," *Chin. J. Laser Med. Surg.* vol. 3, no. 4, pp. 215–217, 1994.

[6] S. Zhao, Y. Gu, P. Xue, J. Guo, T. Shen, T. Wang, N. Huang, L. Zhang, H. Qiu, X. Yu, and X. Wei, "Imaging port wine stains by fiber optical coherence tomography," *J. Biomed. Opt.*, vol. 15, no. 3, Art. no. 036020, 2010.

[7] T. Wang, C. Wang, N. Huang, J. Zhang, Y. Gu, and P. Xue, "Handheld optical coherence tomography device for photodynamic therapy," *Chin. Sci. Bull.*, vol. 57, no. 5, pp. 450–454, Feb. 2012.

[8] C. Wang, T. Huo, J.-G. Zheng, N. Zhang, T. Chen, W. Liao, Y. Wang, Y. Gu, and P. Xue, "Automated assessment of epidermal thickness and vascular density of port wine stains oct image," *J. Innov. Opt. Health Sci.*, vol. 07, no. 01, Jan. 2014, Art. no. 1350052.

[9] T. Marvdashti, L. Duan, S. Z. Aasi, J. Y. Tang, and A. K. E. Bowden, "Classification of basal cell carcinoma in human skin using machine learning and quantitative features captured by polarization sensitive optical coherence tomography," *Biomed. Opt. Express*, vol. 7, no. 9, p. 3721, Sep. 2016.

[10] S. Adabi, S. Conforto, M. Hosseinzadeh, S. Noe, S. Daveluy, D. Mehregan, and M. Nasiriavanaki, "Textural analysis of optical coherence tomography skin images: Quantitative differentiation between healthy and cancerous tissues," *Proc. SPIE*, vol. 10053, Feb. 2017, Art. no. 100533F.

[11] N. Singla, V. Srivastava, and D. S. Mehta, "In vivoclassification of human skin burns using machine learning and quantitative features captured by optical coherence tomography," *Laser Phys. Lett.*, vol. 15, no. 2, Feb. 2018, Art. no. 025601.

[12] W. T. Freeman and M. Roth, "Orientation histograms for hand gesture recognition," in *Proc. Int. Workshop Autom. Face Gesture Recognit.*, vol. 12, 1995, pp. 296–301.

[13] P. P. Srinivasan, L. A. Kim, P. S. Mettu, S. W. Cousins, G. M. Comer, J. A. Izatt, and S. Farsiu, "Fully automated detection of diabetic macular edema and dry age-related macular degeneration from optical coherence tomography images," *Biomed. Opt. Express*, vol. 5, no. 10, p. 3568, Oct. 2014.

[14] E. Mousavi, R. Kafieh, and H. Rabbani, "Classification of dry age-related macular degeneration and diabetic macular edema from optical coherence tomography images using dictionary learning," 2019, *arXiv:1903.06909*. [Online]. Available: https://arxiv.org/abs/1903.06909

[15] F. G. Venhuizen, B. van Ginneken, F. van Asten, M. J. J. P. van Grinsven, S. Fauser, C. B. Hoyng, T. Theelen, and C. I. Sánchez, "Automated staging of age-related macular degeneration using optical coherence tomography," *Investigative Ophthalmol. Vis. Sci.*, vol. 58, no. 4, pp. 2318–2328, 2017.

[16] N. Singla, V. Srivastava, and D. S. Mehta, "*In vivo* classification of human skin burns using machine learning and quantitative features captured by optical coherence tomography," *Laser Phys. Lett.*, vol. 15, no. 2, Feb. 2018, Art. no. 025601.

[17] K. W. Gossage, T. S. Tkaczyk, J. J. Rodriguez, and J. K. Barton, "Texture analysis of optical coherence tomography images: Feasibility for tissue classification," *J. Biomed. Opt.*, vol. 8, no. 3, p. 570, 2003.

[18] M. Sonka, V. Hlavac, and R. Boyle. *Image Processing, Analysis, and Machine Vision*. Boston, MA, USA: Cengage Learning, 2014.

[19] C. A. Lingley-Papadopoulos, M. H. Loew, M. J. Manyak, and J. M. Zara, "Computer recognition of cancer in the urinary bladder using optical coherence tomography and texture analysis," *J. Biomed. Opt.*, vol. 13, no. 2, 2008, Art. no. 024003.

[20] K. I. Laws, "Textured image segmentation," Image Process. INST, Univ. Southern California, Los Angeles, CA, USA, Tech. Rep. USCIPI-940, 1980.

[21] F. Tony, K. M. Ting, and Z.-H. Zhou, "Isolation-based anomaly detection," *ACM Trans. Knowl. Discovery Data*, vol. 6, no. 1, 2012, p. 3.
[22] H. Hotelling, "Analysis of a complex of statistical variables into principal components.," *J. Educ. Psychol.*, vol. 24, no. 6, pp. 417–441, 1933.
[23] M. Mehri, "Texture feature evaluation for segmentation of historical document images," in *Proc. 2nd Int. Workshop Historical Document Imag. Process.* 2013, pp. 102–109.
[24] L. Fei-Fei and P. Perona, "A Bayesian hierarchical model for learning natural scene categories," in *Proc. IEEE Comput. Soc. Conf. Comput. Vis. Pattern Recognit. (CVPR)*, vol. 2, Jun. 2005, pp. 524–531.
[25] Y. Zhao, "Hemoporfin photodynamic therapy for port-wine stain: A randomized controlled trial," *PloS ONE*, vol. 11, no. 5, 2016, Art. no. e0156219.
[26] Q. Xiao, Q. Li, K.-H. Yuan, and B. Cheng, "Photodynamic therapy of port-wine stains: Long-term efficacy and complication in Chinese patients," *J. Dermatol.*, vol. 38, no. 12, pp. 1146–1152, Dec. 2011.
[27] S. Wold, K. Esbensen, and P. Geladi, "Principal component analysis," *Chemometrics Intell. Lab. Syst.*, vol. 2, nos. 1–3, pp. 37–52, 1987.
[28] D. M. J. Tax and R. P. W. Duin, "Support vector data description," *Mach. Learn.*, vol. 54, no. 1, pp. 45–66, Jan. 2004.
[29] W.-C. Chang, C.-P. Lee, and C.-J. Lin, "A revisit to support vector data description," Dept. Comput. Sci., Nat. Taiwan Univ., Taipei, Taiwan, Tech. Rep., 2013.
[30] S. Ai and C. Wang, "Machine-learning classification of port wine stain with quantitative features of optical coherence tomography image," *IEEE Photon. J.*, to be published.

SHENGNAN AI received the B.S. degree in biomedical engineering from Tsinghua University, Beijing, China, in 2014, where she is currently pursuing the Ph.D. degree in physics. Her current research interests include optical coherence tomography, machine learning, and medical image processing.

CHENGMING WANG received the B.S. and Ph.D. degrees in physics from Tsinghua University, Beijing, China, in 2011 and 2018, respectively. His current research interest includes medical image processing, ultra-high speed real-time optical coherence tomography, OCT clinical applications in dentistry, dermatology, oncology, and forensic application using OCT.

WENXIN ZHANG was born in Nanjing, Jiangsu, China, in 1992. She received the B.S. and Ph.D. degrees in physics from the Department of Physics, Tsinghua University, Beijing, China, in 2014 and 2019, respectively. Her current research interest includes optical coherence tomography.

JUI-CHENG HSIEH was born in Hsinchu, Taiwan. He received the B.S. degree in physics from the Department of Physics, Tsinghua University, China, in 2016, where he is currently pursuing the master's degree. His current research interests include optical coherence tomography and biomedical optics.

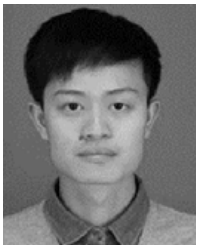

ZHENGYU CHEN was born in Xinyang, Henan, China, in 1997. He received the bachelor's degree in physics from the University of Science and Technology of China, in 2018. He is currently pursuing the degree with Tsinghua University.

BIN HE was born in Jiangxi, China. He received the B.S. degree with the School of Precision Instruments and Opto-Electronics Engineering, Tianjin University, Tianjin, China. He is currently pursuing the Ph.D. degree with the State Key Laboratory of Low Dimensional Quantum Physics, Department of Physics, Tsinghua University. His current research interests include optical coherence tomography (OCT) and digital picture processing.

XIAO ZHANG received the B.S., M.S., and Ph.D. degrees in physics from the College of Applied Sciences, Beijing University of Technology. He is currently an Assistant Professor with the School of Life Science, Beijing Institute of Technology. His research interests include ultrafast laser technology and applications and optical coherence tomography.

NING ZHANG received the Ph.D. degree in physics from Tsinghua University, Beijing, China, in 2014. He is currently an Associate Professor with the Institute of Forensic Science, Ministry of Public Security. His current research interest includes video/image processing, hand-held optical coherence tomography, and forensic applications using OCT.

YING GU was born in Beijing, China, in 1959. She received the B.S. degree from Tianjin Medical University, in 1988, and the M.D. and Ph.D. degrees from the PLA Medical College, in 1988 and 2000, respectively.

She is currently an Academician of the Chinese Academy of Sciences, and a Chief Physician and the Director of the Department of Laser Medicine, PLA General Hospital, China. Her fields of study fall mainly in applications of lasers in surgery and medicine. She established a new type of vascular targeted photodynamic therapy, which became a clinical treatment method for a wide variety of microvascular diseases. She conducted systematic studies of the theory and mechanism, drugs and equipment, technologies and methods, and applications and specifications of vascular targeted photodynamic therapy, guided a new academic direction and created application fields of vascular targeted photodynamic therapy. She collaboratively developed a new pharmaceutical drug for vascular targeted photodynamic therapy. She presided over the formulation of China's first medical laser technical operating specifications and diagnostic guidelines.

PING XUE (Member, IEEE) was born in Jiangxi, China, in 1965. He received the B.S. degree in applied physics and the Ph.D. degree in optics from Tsinghua University, Beijing, China, in 1988 and 1993, respectively.

He was a Lecturer, from 1993 to 1996, and an Associate Professor, from 1996 to 2000, with the Department of Physics, Tsinghua University. From 2001 to 2002, he was a Visiting Scientist with the Research Laboratory of Electronics (RLE), Massachusetts Institute of Technology. Since 2000, he has been a Full Professor with the Department of Physics, Tsinghua University, Beijing, China. From 2002 to 2011, he was the Deputy Director with the Key Laboratory of Atomic and Molecular Nanosciences, Ministry of Education, Tsinghua University. Since 2011, he has been the Deputy Director of the State Key Laboratory of Low-Dimensional Quantum Physics, Tsinghua University, Beijing. He has coauthored two books, more than 150 articles, and more than 25 inventions. His research interests include biomedical imaging, optical coherence tomography (OCT), advanced laser technology, laser spectroscopy, and optical informatics.

Prof. Xue is a member of the Society of Photo-Optical Instrumentation Engineers (SPIE) and the Optical Society of America (OSA). He is an Editorial Board Member of the journal *Chinese Science Bulletin* and the *Journal of Atomic and Molecular Physics*.